Research Square

Preprints are preliminary reports that have not undergone peer review.
They should not be considered conclusive, used to inform clinical practice,
or referenced by the media as validated information.

Plasma-treated L-arginine alters breast cancer cell-derived small extracellular vesicles (sEVs) miR-21 and selectively suppresses cancer cell viability

Liyin DU
Nagoya University
Xizhuo DU
Kunming University of Science and Technology
Yashiro MOTOOKA
Nagoya University Graduate School of Medicine
Kae NAKAMURA
Nagoya University
Camelia MIRON
Nagoya University
Ayako TANAKA
Nagoya University
Masaaki MIZUNO
Nagoya University Hospital
Shinya TOYOKUNI
Nagoya University
Hiroaki KAJIYAMA
Nagoya University
Masaru HORI
Nagoya University
Hiromasa TANAKA
tanaka.hiromasa.g1@f.mail.nagoya-u.ac.jp
Nagoya University

Article

Keywords: cold atmospheric pressure plasma, plasma-treated L-arginine (PTA), breast cancer, selectivity, sEVs, miRNA

Posted Date: November 20th, 2026

DOI: https://doi.org/10.21203/rs.3.rs-11499602/v1

License: This work is licensed under a Creative Commons Attribution 4.0 International License.
Read Full License

Additional Declarations: No competing interests reported.

Plasma-treated L-arginine alters breast cancer cell-derived small extracellular vesicles (sEVs) miR-21 and selectively suppresses cancer cell viability

Liyin DU[1], Xizhuo DU[3], Yashiro MOTOOKA[5,7], Kae NAKAMURA[2,6], Camelia MIRON[2], Ayako TANAKA[2], Masaaki MIZUNO[4], Shinya TOYOKUNI[2,5], Hiroaki KAJIYAMA[2,6], Masaru HORI[2] and Hiromasa TANAKA[1,2]

1 Department of Electronics, School of Engineering, Nagoya University, Nagoya, Japan.
2 Center for Low-temperature Plasma Sciences, Nagoya University, Nagoya, Japan.
3 Medicine Faculty, Kunming University of Science and Technology, Kunming, China.
4 Center for Advanced Medicine and Clinical Research, Nagoya University Hospital, Nagoya, Japan.
5 Department of Pathology and Biological Responses, Nagoya University Graduate School of Medicine, Nagoya, Japan.
6 Department of Obstetrics and Gynecology, Nagoya University Graduate School of Medicine, Nagoya, Japan.
7 Department of Diagnostic Pathology, Fujita Health University, Aichi, Japan.

E-mail: tanaka.hiromasa.g1@f.mail.nagoya-u.ac.jp

Abstract

This study investigated the selective and sustained inhibitory effects of plasma-treated L-arginine (PTA) on breast cancer cells and explored the potential involvement of small extracellular vesicle (sEV)-mediated intercellular communication. PTA selectively reduced the viability of MCF-7 breast cancer cells compared with MCF-10A normal mammary epithelial cells. To examine whether vesicle-associated signaling contributes to this sustained response, sEVs were isolated from untreated and PTA-treated MCF-7 cells and characterized by nanoparticle tracking analysis, transmission electron

microscopy, cellular uptake imaging, and functional assays. sEVs derived from PTA-treated MCF-7 cells retained typical vesicle-like morphology and were efficiently internalized by recipient cells. Functionally, these sEVs selectively suppressed MCF-7 cell viability while exerting limited effects on MCF-10A cells. miRNA analysis further showed that miR-21 expression was decreased by approximately 68% in sEVs derived from PTA-treated MCF-7 cells compared with untreated controls. These findings suggest that PTA may exert sustained anticancer effects, at least in part, by altering cancer cell-derived sEV cargo and modulating vesicle-mediated intercellular signaling. This study provides a potential link between plasma-activated amino acid treatment and sEV-associated regulation of breast cancer cell viability.

Keywords: cold atmospheric pressure plasma, plasma-treated L-arginine (PTA), breast cancer, selectivity, sEVs, miRNA

1. Introduction

In 2020, approximately 2.3 million new cases of breast cancer were diagnosed worldwide, making it the most frequently diagnosed cancer among women [1]. Current therapeutic strategies for breast cancer mainly include surgery, chemotherapy, radiotherapy, and targeted therapy. Although significant advances have been achieved in recent years, there remains a strong need to develop therapeutic approaches that are cost-effective, readily accessible, highly selective toward cancer cells, and associated with minimal side effects.

To address these challenges, cold atmospheric pressure plasma (CAP)-based

therapies have emerged as a promising alternative strategy. For example, plasma jets have been applied in the treatment of head and neck cancers [2]. In addition, plasma-activated liquids, such as plasma-activated medium (PAM) and plasma-activated Ringer's lactate (PAL), have demonstrated significant selective cytotoxicity toward cancer cells. These plasma-activated solutions were reported to effectively reduce the viability of human brain tumor cells (U251SP) while causing minimal damage to normal astrocytes (ACBRI-371) [3].

As an indirect application of CAP, plasma-activated solutions offer several advantages compared with direct plasma treatment. Because they are in liquid form, their chemical composition and reactive species can be quantitatively analyzed using various analytical techniques. This property enables a more comprehensive investigation of the underlying chemical mechanisms and facilitates future clinical evaluations regarding safety and dosage control.

It is widely recognized that interactions between the plasma gas phase and the liquid interface generate a complex mixture of reactive oxygen and nitrogen species (RONS), which are considered the key factors responsible for the selective anti-tumor effects of plasma-activated solutions [4], [5]. Mechanistic studies have revealed that RONS-induced oxidative stress can trigger multiple cellular responses. On the one hand, RONS can directly damage the phospholipid bilayer of cell membranes, leading to compromised membrane integrity and subsequent cell death [6]. On the other hand, RONS-induced endoplasmic reticulum stress can promote calcium influx into mitochondria, resulting in the loss of mitochondrial membrane potential and activation

of mitochondria-dependent apoptosis pathways. These processes are often accompanied by the modulation of the PI3K–Akt signaling pathway and the upregulation of stress-responsive genes, including GADD45α/β, ATF3, and c-JUN [7]. Similarly, PAL has been shown to induce apoptosis in glioblastoma cells through the downregulation of c-FOS and c-JUN, as well as the suppression of downstream targets within the YAP–TEAD signaling pathway, such as c-MYC, CTGF, and CYR61 [8]. These intracellular signaling events collectively contribute to the selective cytotoxicity of plasma-activated solutions toward cancer cells while minimizing damage to normal cells.

In this study, an aqueous solution of L-arginine·HCl was selected as the precursor for the preparation of plasma-treated L-arginine (PTA) using CAP. L-arginine is a non-essential amino acid commonly used as a supplement in cell culture media and has not been reported to exhibit cytotoxic effects. Compared with most other amino acids, L-arginine contains four nitrogen atoms in its molecular structure (Figure 1), which may serve as an efficient source for the generation of nitrogen-containing reactive species. In addition, L-arginine is known to participate in various immune-related physiological processes [9], [10], and has been reported to play a role in adjuvant cancer therapy. Supplementation with L-arginine can promote T-cell proliferation and enhance their effector functions, particularly in $CD8^+$ cytotoxic T lymphocytes and natural killer cells [11].

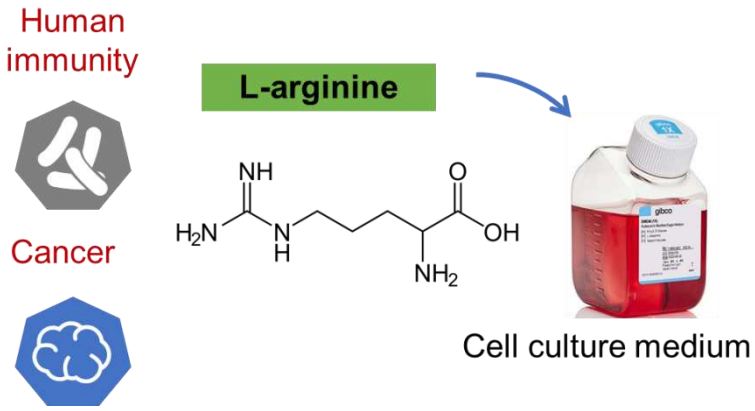


Figure 1. L-arginine molecular structure and functions.

Our previous studies demonstrated that PTA exhibits selective cytotoxicity toward breast cancer cells at appropriate dilution ratios [12], [13]. Interestingly, we observed that PTA initially induced apoptosis within several hours after treatment. However, although the dominant mode of cell death changed at later time points, the viability of MCF-7 cells remained suppressed for up to 96 h. This observation suggests that the selective inhibitory effect of PTA may involve multiple mechanisms, which will be further discussed in Section 2.4 and Section 3.2.

Small extracellular vesicles (sEVs) are lipid bilayer-enclosed particles released by cells and are typically enriched in vesicles ranging from approximately 30 to 200 nm in diameter. They carry diverse molecular cargo, including proteins, miRNAs, mRNAs, and DNA, and thereby participate in intercellular communication by transferring biological information to recipient cells [14], [15]. Because vesicle biogenesis, secretion, and uptake occur over a time scale that may overlap with the sustained inhibitory effects observed after PTA treatment, sEV-mediated signaling may provide a potential mechanism linking the initial plasma-induced response to prolonged

changes in cancer cell viability. Although increasing evidence supports the anticancer potential of plasma-activated solutions, the mechanisms underlying their sustained and selective effects remain incompletely understood. In particular, whether plasma-activated amino acid solutions alter cancer cell-derived sEV cargo and thereby influence vesicle-mediated communication has not yet been fully clarified.

The aim of this study was to investigate the sustained inhibitory effect of plasma-treated L-arginine (PTA) on breast cancer cells and to explore the potential involvement of sEV-mediated signaling in this process. By considering the temporal dynamics of PTA-induced cytotoxicity together with vesicle secretion and uptake, we analyzed the characteristics and functional effects of sEVs derived from untreated and PTA-treated MCF-7 cells. Furthermore, the expression levels of selected sEV-associated miRNAs were examined to identify potential regulatory molecules associated with PTA-induced selective inhibition.

2. Methods and materials

2.1 Prepareation of plasma-treated L-arginine (PTA)

The plasma source equipment (Fuji Co., Ltd., Aichi, Japan) was equipped with a purge system. This system used a 300-second pulse of argon (Ar) gas to reduce the O_2 level to below 0.2% while maintaining the set stable gas ratio. The plasma was generated using a 9 kV, 60 Hz AC power supply to ignite a gas mixture with a volume ratio of 8:1:1 for Ar, N_2, and O_2. The total gas flow rate was 2 slm. The distance between the plasma nozzle and the surface of the sample liquid was set to L = 19 mm, and the

irradiation time was 5 minutes, consistent with previous studies[12], [18], [19], [20], [21]. The equipment was set as Figure 2.

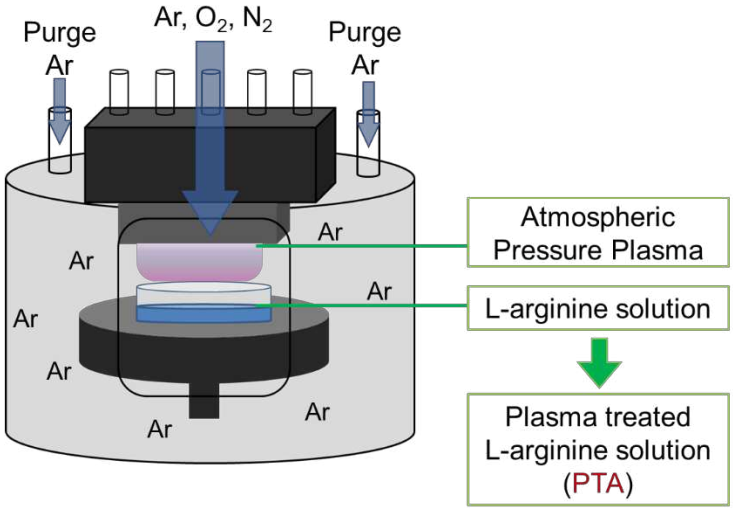


Figure 2. Equipment used for PTA preparation. The metal chamber was equipped with a gas-purging system to reduce the oxygen concentration to below 0.2%.

A solution of 474.7 mM was prepared by dissolving 1 g of L-arginine·HCl, ($C_6H_{14}N_4O_2$·HCl, Peptide Institute, Inc., Osaka, Japan) in 10 mL of ultrapure water. PTA solutions were produced by irradiating the L-arginine solutions with the Ar/O_2/N_2 plasma for 5 minutes to get PTA474. The number following PTA clarified the initial concentration of L-arginine solution.

2.2 Cell lines and culture

MCF-7 (human breast cancer cell line) and MCF-10A (normal human mammary epithelium cell line) were purchased from the American Type Culture Collection (ATCC, Manassas, USA).

MCF-7 cells were cultured in Dulbecco's Modified Eagle Medium (DMEM;

D5796; Millipore/Sigma-Aldrich, USA) supplemented with 10% FBS (ThermoFisher, USA) and 1% Penicillin-Streptomycin (P/S; stock solution containing 10,000 units/mL penicillin and 10,000 µg/mL streptomycin; ThermoFisher Scientific/Life Technologies, Grand Island, NY, USA).

MCF-10A cells were cultured in medium prepared using the Mammary Gland Epithelial Cell Growth Medium Bullet Kit (MEGM; Catalog No. CC-3150; Lonza, Basel-Stadt, Switzerland), with the addition of 100 nanograms per milliliter (ng/mL) of cholera toxin (Catalog No. 030-20621; Wako Chemical Co., Ltd., Osaka, Japan). Both cell lines were incubated at 37 °C in a humidified atmosphere containing 5% CO_2 and were passaged at approximately 80% confluence (Figure 3), as detailed in our previous work [13], [18], [22], [23].

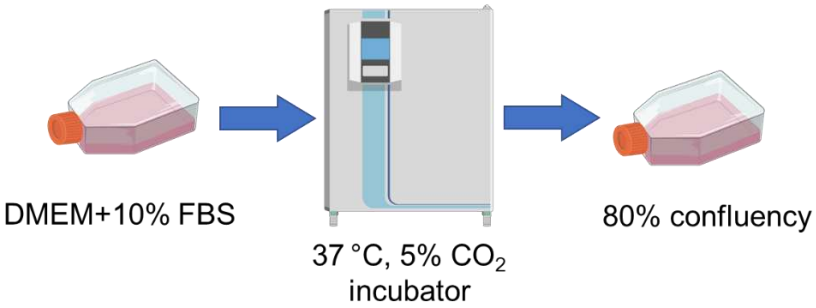


Figure 3. Cell culture method

2.3 Measurement of cell viability

Cells were seeded at a density of 5,000 cells per well in 96-well plates. After 24 h of growth in complete DMEM (DMEM (+)), the medium was then replaced with 200 µL of serially diluted PTA in basal DMEM (DMEM(-)), which provided an appropriate osmotic environment for cell survival.

Cells were incubated for an additional 24, 48, 72, or 96 h. Cell viability after PTA treatment or sEVs exposure was assessed using the CellTiter 96® Aqueous One Solution Cell Proliferation Assay Kit (Promega, Madison, WI, USA) according to the manufacturer's protocol.

2.4 Cell apoptosis detection

Cell apoptosis was assessed using the CellEvent™ Caspase-3/7 Detection Reagent (Thermo Fisher Scientific, C10423, USA). Cells were seeded in an 8-well chambered glass slide (Corning Inc., 354118, USA) at a density of 20,000 cells per well and incubated in a humidified incubator. After 24 h, the cells were treated with gradient-diluted PTA solutions for 2 h.

Following treatment, the Caspase-3/7 detection reagent was added to each well at a final concentration of 5 μM and incubated for 1 h. The cells were then observed using an inverted fluorescence microscope (Olympus, DP80, Japan). The procedures are shown as Figure 4.

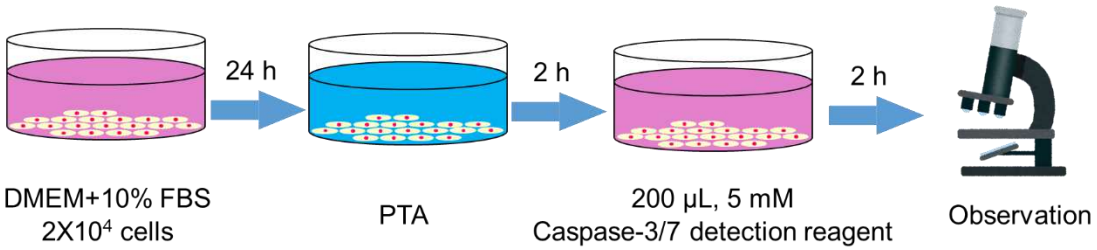


Figure 4. Cell apoptosis detection.

2.5 sEVs extraction

sEVs were isolated following the procedure illustrated in Figure 5. Cells were

cultured in complete medium in cell culture flasks until approximately 80% confluence. The culture medium was then removed, and the cells were treated with a 300-fold diluted PTA solution for 2 h.

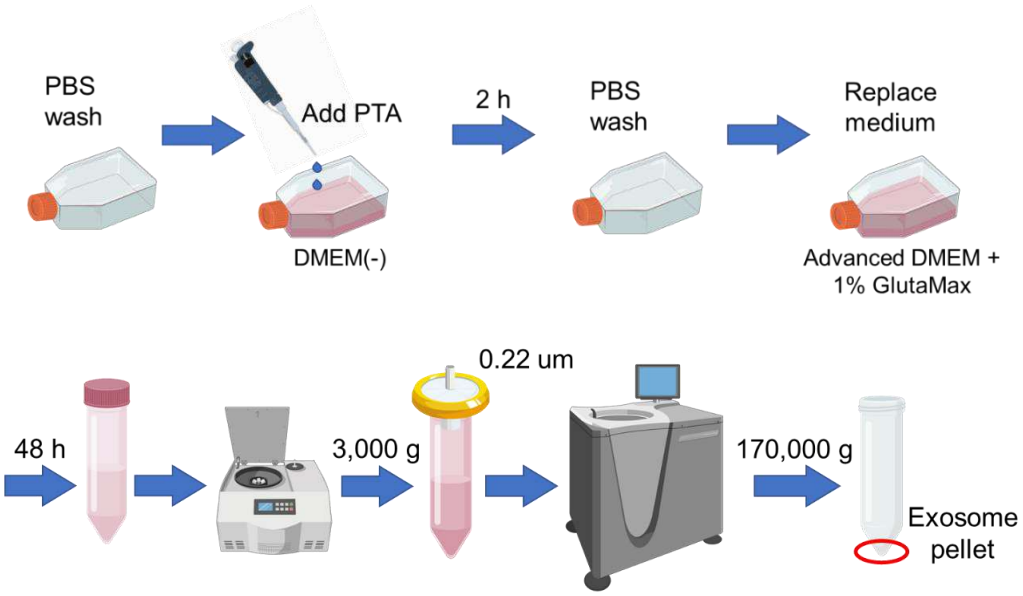


Figure 5. sEVs extraction process.

After treatment, the cells were gently washed three times with PBS and cultured in Advanced DMEM (Thermo Fisher Scientific, 12491015, USA) supplemented with 1% GlutaMAX (Thermo Fisher Scientific, 35050061, USA). After 48 h of incubation, the culture supernatant was collected.

Cell debris and large vesicles were removed by centrifugation, followed by filtration through a 0.22 μm filter to eliminate bacteria. The filtered supernatant was then ultracentrifuged at 170,000 × g for 70 min. The resulting pellet was washed once with PBS and subjected to a second ultracentrifugation under the same conditions. Finally, the sEVs pellet was resuspended in PBS and stored at −80 °C until further analysis.

2.6 sEVs size characterization

SEV samples (10 μL) were diluted with 990 μL of PBS to obtain a final volume of 1 mL for size distribution analysis. The particle size and concentration of sEVs were measured using nanoparticle tracking analysis (NTA) with a NanoSight NS300 instrument (Malvern Panalytical Ltd., Malvern, UK) as shown in Figure 6.

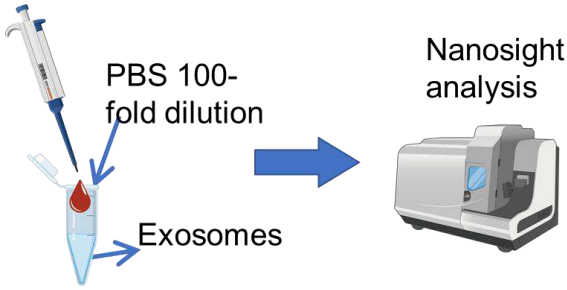


Figure 6. sEV particle size and distribution analysis.

After the particle count stabilized, video recording was initiated. Five videos of 60 s each were captured for every sample, and the analysis report was automatically generated by the instrument software after recording was completed.

2.7 sEV morphology characterization

A 200-mesh copper grid (Sigma-Aldrich, G4776, USA) was exposed to glow-discharge plasma for 30 s to improve its hydrophilicity and enhance the attachment of sEV sample droplets. Drops of the sEV sample and 2% uranyl acetate staining solution were placed on the surface of a hydrophobic substrate.

The plasma-treated copper grid was inverted onto the sEV sample droplet for 10 s

and then transferred to the 2% uranyl acetate solution for negative staining, as illustrated in Figure 7. Finally, the grid was observed using a JEM-1400Plus transmission electron microscope (TEM) (JEOL Ltd., Tokyo, Japan).

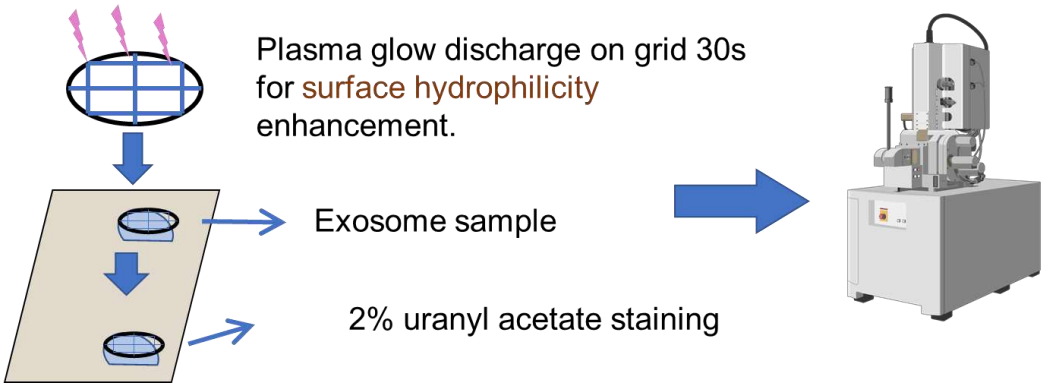


Figure 7. sEV morphology observation method.

2.8 sEV function validation

To verify the functional effects of sEVs derived from the breast cancer cell line MCF-7, a cell viability assay similar to the MTS assay described in Section 2.3 was performed.

Cells were seeded at a density of 5,000 cells per well in 96-well plates and cultured in complete medium for 24 h to allow cell attachment. The wells were then gently washed three times with PBS to remove sEVs originating from fetal bovine serum (FBS) in the complete medium.

sEVs (80 μg, based on total protein content) were added to each well. After incubation for a specified period, cell viability was measured using a microplate reader. The experimental procedure is illustrated in Figure 8.

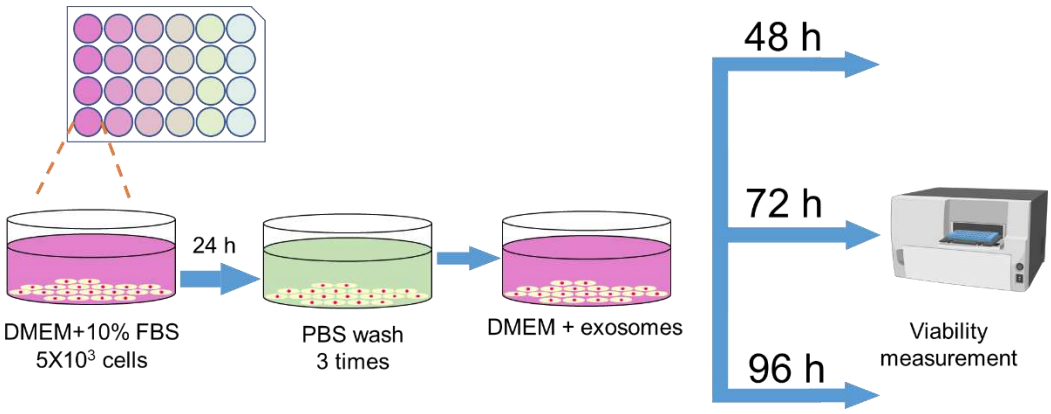


Figure 8. sEV function validation method.

2.9 Fluorescence staining

To confirm that sEVs entered cells during their functional activity, fluorescence staining of sEVs and cells was performed. Since sEVs and cell membranes share similar lipid bilayer structures, both can be stained with lipid dyes. Therefore, the lipid dye PKH26 was used to label sEVs, while F-actin staining was used to visualize the cell outline.

sEV samples (20 μL) were mixed with 4 μL PKH26 (Sigma-Aldrich, 12352207, Germany). After 5 min of incubation, sEV-depleted FBS (SBI, EXO-FBS-50A-1, USA) was added to bind excess dye and terminate the staining reaction. The supernatant containing free dye was removed by ultracentrifugation.

The PKH26-labeled sEVs were then added to 8-well chamber slides co-cultured with cells at 20,000 cells per well. After 6 h of co-culture, the slides were gently washed three times with PBS to remove unbound labeled sEVs. Cells were fixed with 4% paraformaldehyde (PFA) (Fujifilm, 161-20141, Japan) for 10 min, followed by blocking with a buffer containing 5% normal goat serum and 1% BSA for 1 h.

Phalloidin was then added to stain F-actin for 1 h. After removing all staining solutions, 8 μL of DAPI was added, and the slides were cover-slipped. The samples were then observed using an inverted fluorescence microscope. The entire procedure is illustrated in Figure 9.

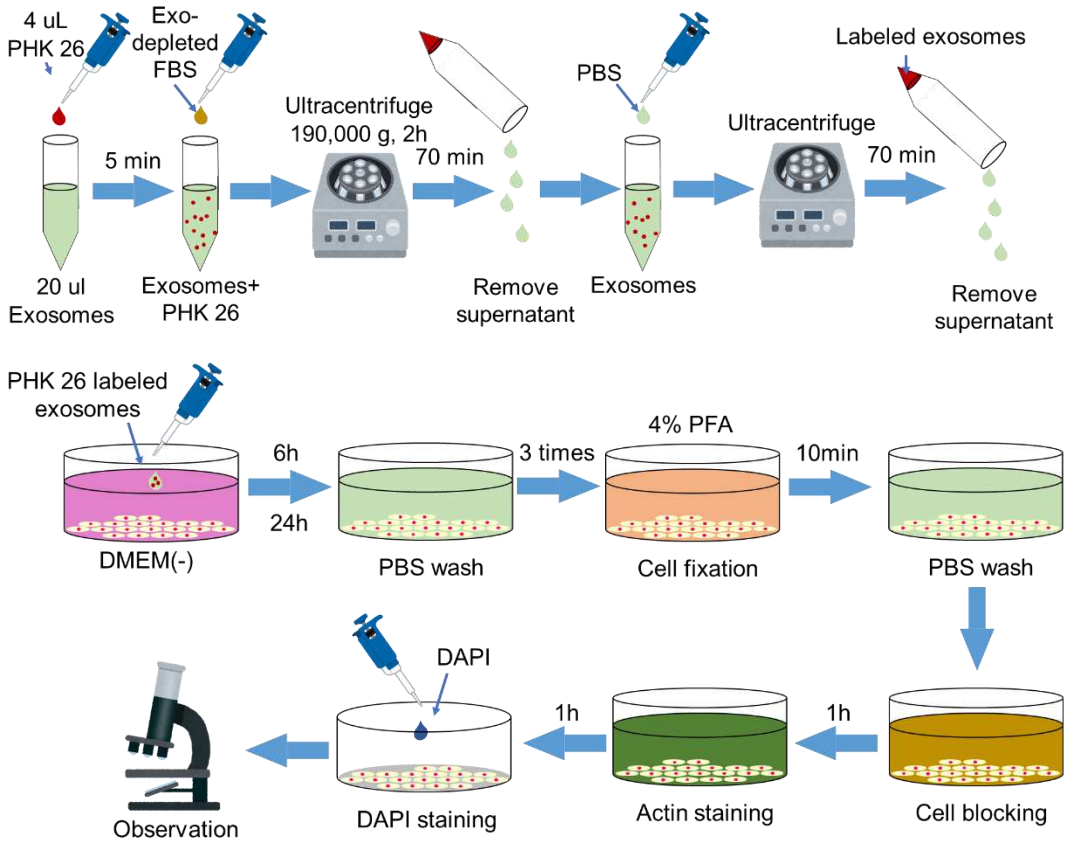


Figure 9. sEV, F-actin and cell nucleus triple staining.

2.10 qRT-PCR

miRNAs in sEVs were extracted using the miRNeasy Kit (Qiagen, 217084, Germany). The concentration of extracted miRNAs was measured using the Qubit microRNA Assay Kit (Thermo Fisher, Q32880, USA) according to the manufacturer's instructions. The expression levels of miR-21, miR-34a, and miR-200c in the sEV samples were analyzed by qRT-PCR, using U6 as the reference RNA.

cDNA was synthesized from 5 μg of miRNA using the TaqMan Advanced miRNA cDNA Synthesis Kit (Thermo Fisher, A28007, USA) according to the manufacturer's protocol. qRT-PCR reactions were conducted using TaqMan Fast Advanced Master Mix (Thermo Fisher, 4444557, USA). The thermal cycling conditions were as follows: initial denaturation at 95 °C for 5 min, followed by 40 cycles of 95 °C for 10 s and 60 °C for 30 s. The relative expression levels of the target miRNAs were calculated using the $2^{-\Delta\Delta Ct}$ method.

2.11 Statistical analysis

All cell viability assays were independently performed with six replicate wells per group (n = 6). Due to the limited yield of isolated sEVs, sEV function validation experiments were conducted with four replicate wells per group (n = 4).

Experimental data are presented as mean ± standard deviation (SD). Data organization and figure preparation were performed using Microsoft Excel and Origin (OriginLab, USA). Statistical significance was defined as $p < 0.05$.

3. Results

3.1 Selective and sustained inhibitory effect of PTA474

The MTS assay was performed to evaluated the cytotoxic effect of PTA474 on breast cancer cells. At an appropriate dilution ratio (64-fold), PTA474 significantly reduced the viability of MCF-7 cells to 44.9%, while the viability of normal mammary epithelial cell MCF-10A was not damaged, indicating a pronounced selective cytotoxic

effect in Figure 10a.

In addition, this selective inhibitory effect was sustained over 72 h, suggesting that PTA474 maintained long-lasting cytotoxic activity against cancer cells (Figure 10b).

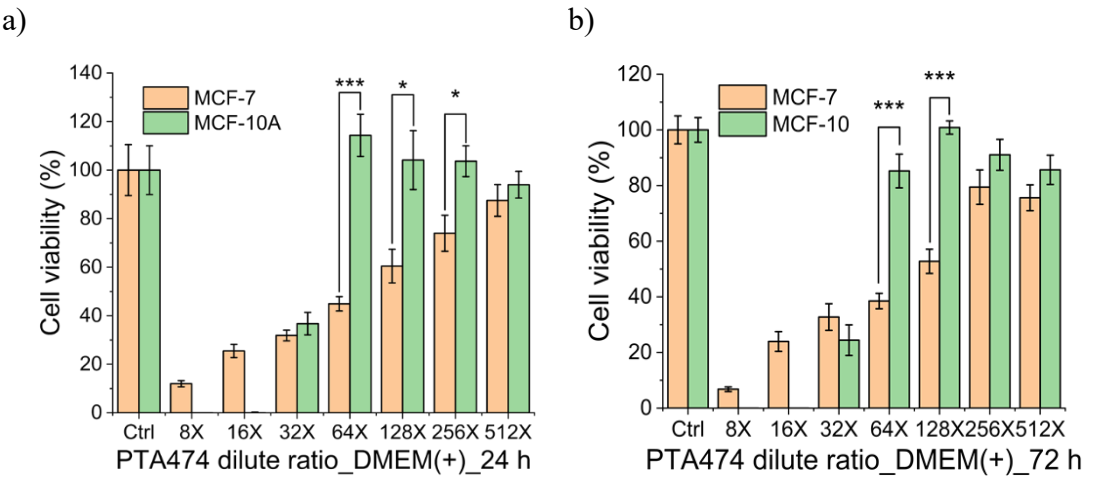


Figure 10. Selective and sustained inhibitory effect of PTA474 on breast cancer cells.

3.2 Cell apoptosis

Section 3.1 has shown that cells were selectively killed following treatment with PTA solutions. To further investigate whether this effect was associated with apoptosis, a caspase-3/7 detection reagent was used to evaluate apoptotic activity. As shown in Figure 11, the green fluorescence signal represents the activation of caspase-3/7 and therefore indicates the level of apoptosis. Images in Figure 11a–11d were obtained 2 h after PTA treatment, and Figure 11e–11h were recorded 24 h after treatment.

After 2 h of incubation, strong green fluorescence was observed in the PTA-treated groups, particularly at the 64-fold dilution, indicating a pronounced induction of apoptosis. Moreover, the fluorescence intensity showed a positive correlation with PTA concentration, suggesting that apoptosis induction was concentration-dependent

(Figure 11a–11d).

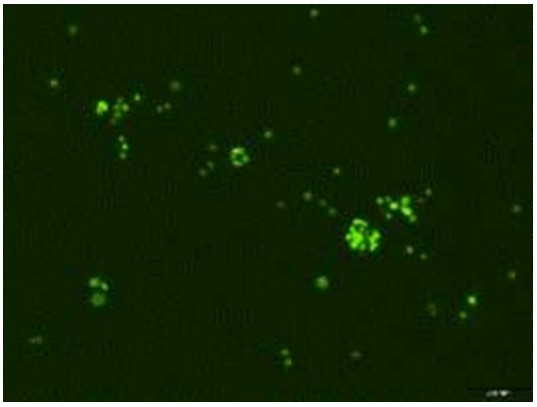
However, after 24 h of treatment, the fluorescence signal was markedly reduced. Only a small number of cells exhibited detectable green fluorescence, and no clear relationship between fluorescence intensity and PTA concentration was observed (Figure 11e–11h).

These results indicate that PTA treatment can induce apoptosis within several hours after exposure, but this apoptotic response is transient. The fluorescence signal was visibly weaker at 24 h than at 2 h, suggesting that caspase-3/7 activation was more prominent at the earlier time point. In particular, the inhibitory effect observed after 24 h is likely not primarily mediated by apoptosis.

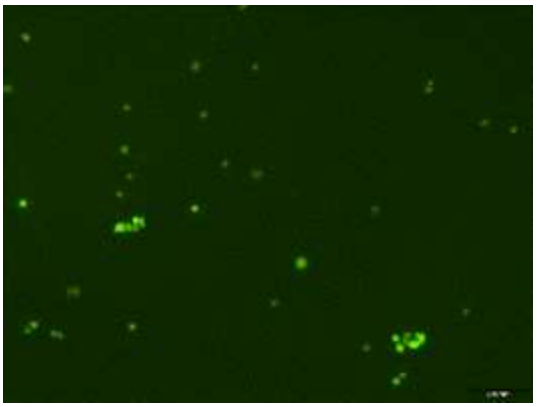
a)



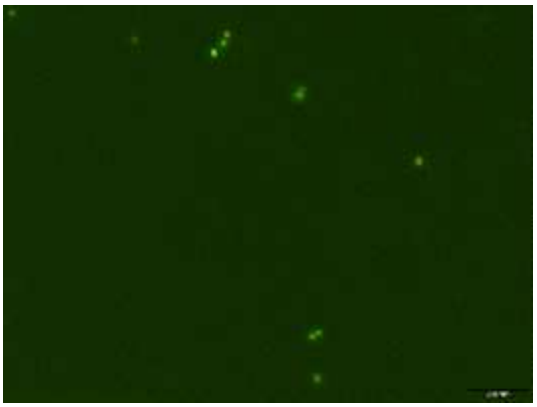
b)



c)



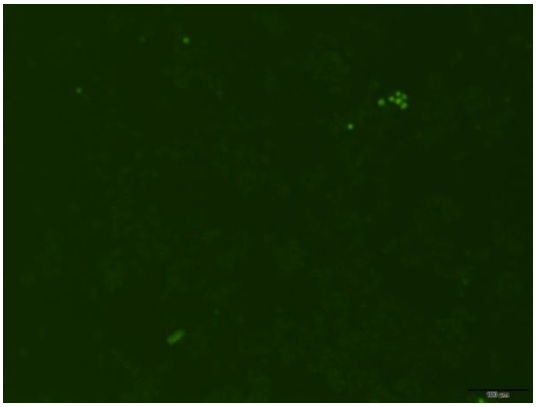
d)



e)



f)



g) h)

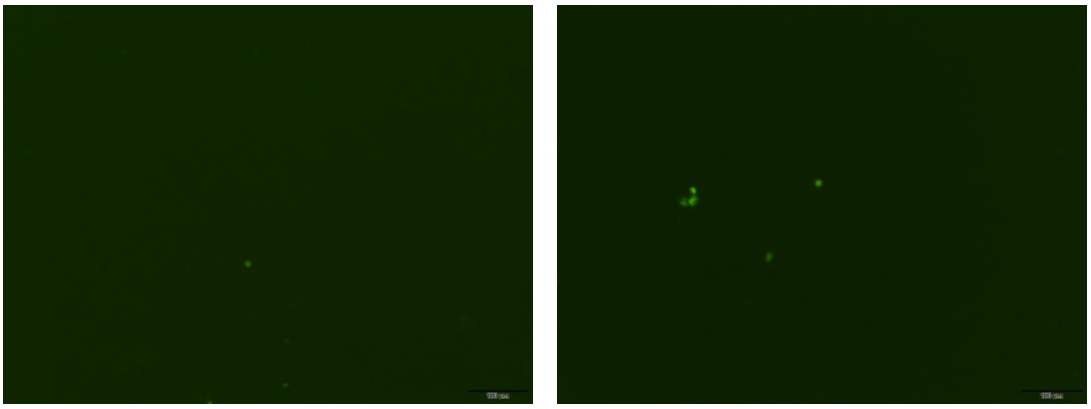


Figure 11. Apoptosis detection in MCF-7 cells after PTA474 treatment using a caspase-3/7 detection reagent. a) Control group of PTA474 after 2 h, b) 64-fold diluted PTA474 after 2 h, c) 128-fold diluted PTA474 after 2 h, d) 256-fold diluted PTA474 after 2 h, e) Control group of PTA474 after 24 h, f) 64-fold diluted PTA474 after 24 h, g) 128-fold diluted PTA474 after 24 h, and h) 256-fold diluted PTA474 after 24 h.

3.3 sEV size and distribution characterization

In this research, the sEVs extracted from the PTA-treated MCF-7 cells (PTA-sEVs) and untreated MCF-7 cells (Ctrl-sEVs) were compared. According to the NTA report, the average diameter of Ctrl-sEVs was 167.4 nm. After PTA treatment of MCF-7 cells, the average diameter of PTA-sEVs slightly increased to 179.7 nm. Both groups exhibited particle sizes within the typical sEV range (30–200 nm).

The size distribution profiles of both Ctrl-sEVs and PTA-sEVs are shown in Figure 12. Despite the slight difference in average particle size, the overall size distribution patterns were comparable between the two groups, indicating that PTA treatment did not significantly alter the size characteristics of sEVs released by MCF-7 cells.

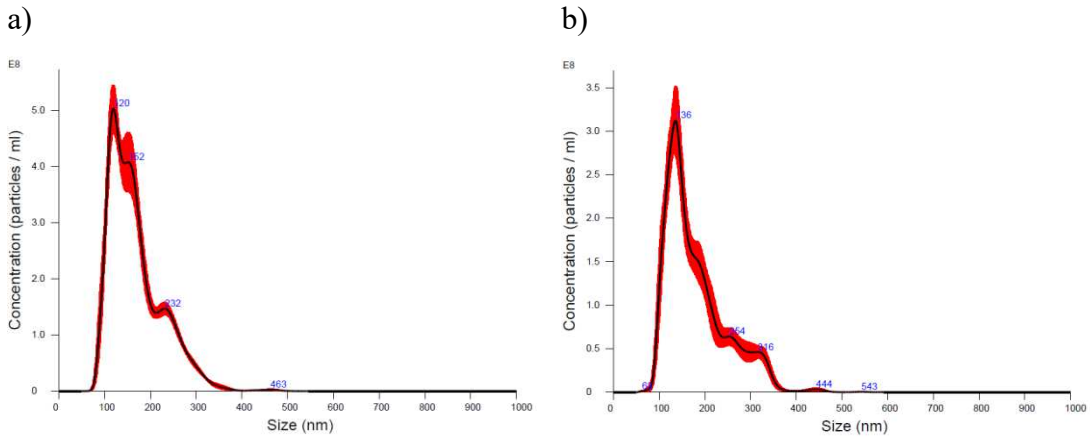


Figure 12. sEV size and distribution. a) Ctrl-sEVs, b) PTA-sEVs

3.4 Ultrastructural characterization of sEVs

TEM was used to examine the morphology of sEVs derived from untreated and PTA-treated MCF-7 cells. Representative TEM images are shown in Figure 13a and 13b. Both Ctrl-sEVs and PTA-sEVs exhibited rounded or cup-shaped vesicle-like morphology, and the observed particle sizes were generally consistent with the NTA results.

These observations suggest that PTA treatment did not noticeably alter the overall morphology of the isolated sEVs.

a) b)

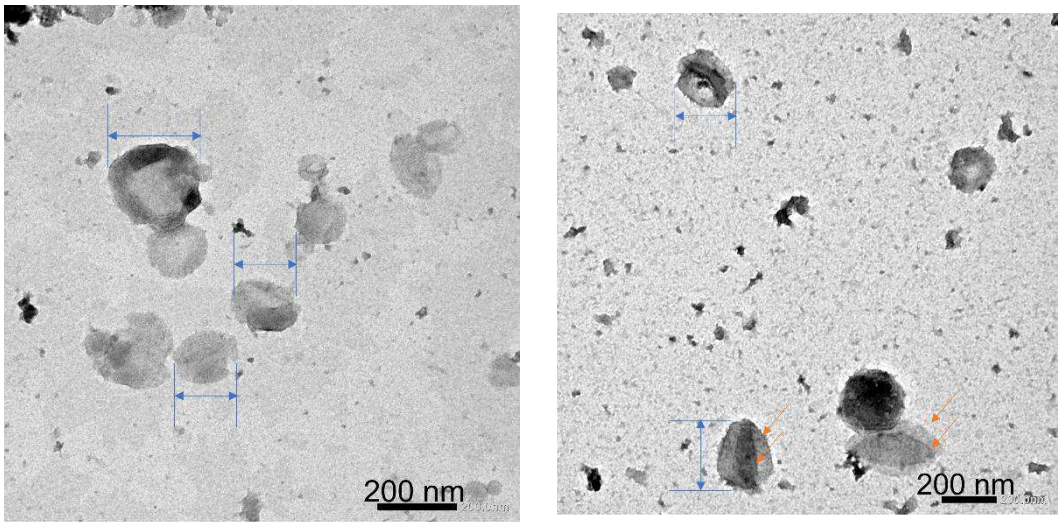


Figure 13. sEV morphology observed by TEM. a) Ctrl-sEVs, b) PTA-sEVs.

3.5 Effects of PTA-derived sEVs on cell viability

The biological effects of Ctrl-sEVs and PTA-sEVs were evaluated using an MTS-based cell viability assay. sEVs were added to MCF-7 and MCF-10A cells, and cell viability was measured after co-culture. To better clarify the endpoint effect of sEV treatment, cell viability at 96 h was further analyzed using the untreated control group of each cell line as 100%.

As shown in Figure 14, at 96 h, Ctrl-sEVs significantly increased the viability of both MCF-7 and MCF-10A cells, suggesting that sEVs derived from untreated MCF-7 cells exerted a pro-proliferative effect on recipient cells. In contrast, PTA-sEVs reduced MCF-7 cell viability to 75.6%, while MCF-10A cell viability remained comparable to the untreated control. These results indicate that PTA treatment altered the biological function of cancer cell-derived sEVs, resulting in selective suppression of breast cancer cell viability without significantly affecting normal mammary epithelial cells.

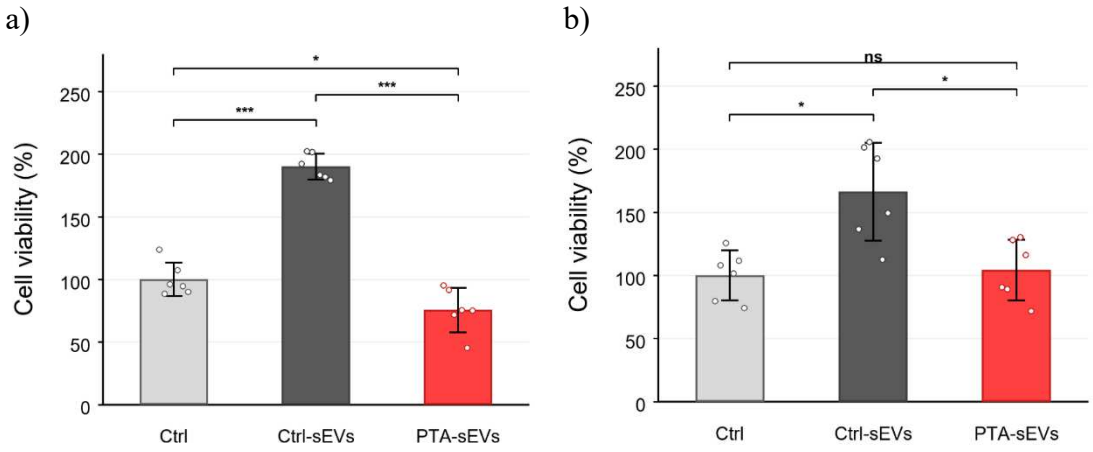


Figure 14. Effects of sEVs on cell viability at 96 h. a) MCF-7 cells and b) MCF-10A cells after co-culture with Ctrl-sEVs or PTA-sEVs for 96 h.

3.6 sEV uptake by cells

The biological effects of sEVs were evaluated through co-culture experiments. To confirm that these effects were mediated by sEV uptake, fluorescence staining was performed to visualize the interaction between sEVs and cells. Triple staining of sEVs (red, PKH26), F-actin (green), and cell nuclei (blue, DAPI) was conducted to observe the relative localization of sEVs within cells. The control group (Ctrl) represents wells without sEVs.

These observations in Figure 15 indicate that sEVs can be effectively taken up by both cell types, supporting the results of the cell viability assays and suggesting that the observed biological effects are mediated through sEV uptake.

a)

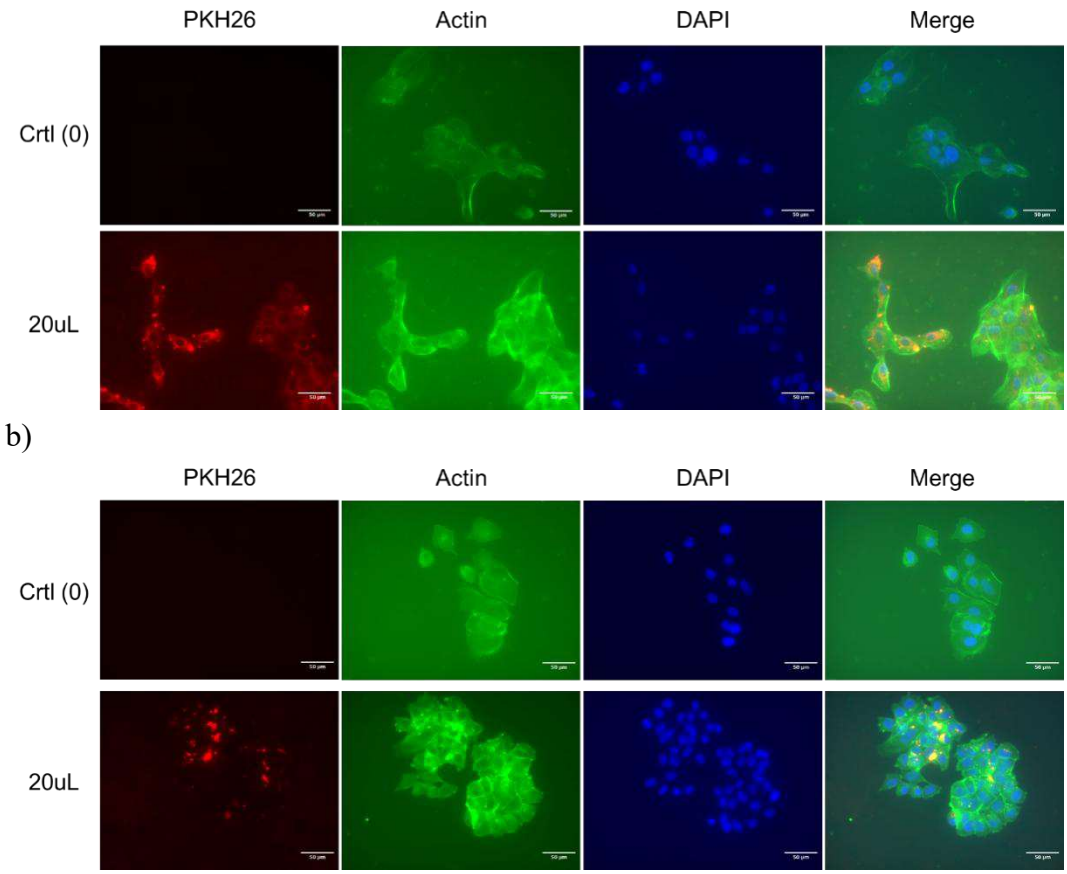


Figure 15. Uptake of PKH26-labeled sEVs by recipient cells. a) MCF-10A cells, b) MCF-7 cells. Red: PKH26-labeled sEVs; green: F-actin; blue: nuclei.

3.7 miR-21 downregulated expression level

The expression levels of several oxidative stress–related miRNAs, including miR-34a, miR-200c, and miR-21, were analyzed in Ctrl-sEVs and PTA-sEVs using qRT-PCR. U6 was used as the internal reference gene.

Among the analyzed miRNAs, miR-21 exhibited a significant decrease in expression in PTA-sEVs compared with Ctrl-sEVs. The relative expression levels of miR-21 are shown in Figure 16.

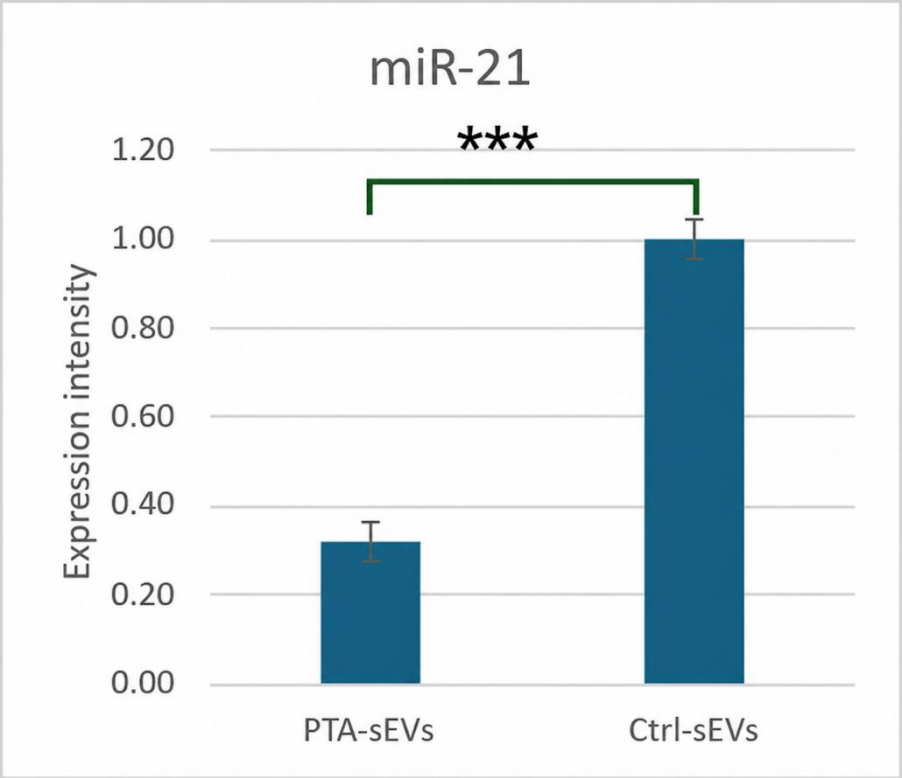


Figure 16. Expression levels of miR-21 in different sEVs

Quantitative analysis showed that the ΔCt value of miR-21 in PTA-sEVs was −23.45, while in Ctrl-sEVs it was −25.09, resulting in a ΔΔCt of 1.64. According to the $2^{-\Delta\Delta Ct}$ method, the relative expression level of miR-21 in PTA-sEVs was approximately 0.32-fold of that in Ctrl-sEVs, corresponding to a 3.1-fold downregulation.

miR-21 is a well-characterized oncogenic miRNA that is commonly overexpressed in various cancers, promoting mitosis, driving cell proliferation, and inhibiting apoptosis [24]. The observed downregulation of miR-21 in PTA-sEVs may contribute to the reduced viability of MCF-7 cells observed in the sEV co-culture experiments.

4 Discussion

Previous studies have extensively investigated the dose-dependent effects of plasma treatment and reactive oxygen and nitrogen species (RONS)-mediated signaling pathways [25], [26], [27]. However, most studies on plasma- or drug-induced gene expression alterations have primarily focused on whole-cell transcriptional responses [28], [29], [30], while relatively limited attention has been paid to cell-to-cell communication mechanisms, particularly those mediated by extracellular vesicles.

In the present study, we observed that PTA solution at an appropriate dilution ratio exhibited a significant and sustained inhibitory effect on the breast cancer cell line MCF-7. By analyzing the expression levels of several oxidative stress–related miRNAs in sEVs, we further explored the potential influence of PTA stimulation on tumor microenvironment regulation and long-distance intercellular communication. These findings help bridge the gap between single-cell biological responses and microenvironmental regulation, and provide a potential perspective for future gene therapy target selection, clinical safety evaluation, and strategies to overcome drug resistance.

Among the investigated miRNAs, miR-21 was significantly downregulated in sEVs derived from PTA-treated cells (PTA-sEVs). miR-21 is a well-characterized oncogenic miRNA that regulates multiple downstream targets involved in tumor proliferation, apoptosis, and metastasis. However, the detailed downstream regulatory pathways associated with the observed miR-21 downregulation were not directly investigated in this study.

Previous studies have shown that miR-21 downregulation can lead to the upregulation of several tumor-suppressive genes, including SPRY2 [24], PTEN [31], TIMP3 [32], BCL2 [33], and PDCD4 [34]. For example, the restoration of SPRY2 expression has been reported to regulate the intracellular trafficking of EGFR and HER2 within the endosomal system, thereby negatively modulating the PI3K/AKT/mTOR signaling pathway. SPRY2 can also suppress the ERK/MAPK signaling pathway through inhibition of Raf1 [35].

The PI3K/AKT/mTOR signaling pathway plays a critical role in cancer progression by inhibiting apoptosis, promoting glycolysis, and altering cellular energy metabolism, thereby supporting cancer cell survival under hypoxic conditions [36]. Meanwhile, the ERK/MAPK signaling pathway contributes to sustained cell division and rapid tumor proliferation [37]. Therefore, restoration of SPRY2 expression may contribute to correcting abnormal proliferative signaling and slowing tumor growth.

In addition to SPRY2, PTEN, another well-known target of miR-21, can negatively regulate the PI3K/AKT/mTOR signaling pathway by suppressing AKT activation [38]. Similarly, RECK can inhibit the activity of matrix metalloproteinases MMP-2 and MMP-9, thereby reducing tumor invasiveness [39], [40]. These metalloproteinases are frequently overexpressed in cancer cells and are closely associated with tumor invasion and metastasis [41], [42].

TIMP3 has been reported to negatively regulate ADAM10 and ADAM17, which are often overexpressed in cancer cells and participate in the activation of multiple

signaling pathways, including those involving Notch receptors, transforming growth factor β (TGF-β), HER2, HER4, and VEGFR2 [43].

Downregulation of miR-21 can also reduce its interaction with the 3′-UTR region of the BCL2 gene, thereby altering the BAX/BCL2 expression ratio, which is a key regulator of apoptosis [33], [44], [45]. In addition, PDCD4 has been reported to negatively regulate the JNK signaling pathway, which may lead to decreased BCL2 protein expression and further influence apoptosis regulation [46].

All these findings above suggest that the downregulation of exosomal miR-21 induced by PTA treatment may contribute to the selective inhibition of breast cancer cells. One possible explanation is that the RONS generated during plasma treatment influence intracellular miRNA regulation or the sorting of miRNAs into sEVs. Through this process, PTA stimulation may alter sEV-mediated cell-to-cell communication, thereby affecting cancer cell proliferation and survival.

Several limitations should be noted in this study. First, although the downregulation of miR-21 in PTA-sEVs was observed, the downstream signaling pathways and target gene expression were not experimentally verified. Second, the experiments were performed using in vitro cell models, and the biological effects of PTA-modified sEVs in in vivo tumor environments remain unclear. Further studies will be required to investigate the molecular mechanisms of miRNA regulation and the therapeutic potential of plasma treatment-modified sEVs in cancer treatment.

5 Conclusion

In this research, the biological effects of plasma-treated L-arginine (PTA) solution on breast cancer cells were investigated. PTA treatment exhibited a selective and sustained inhibitory effect on MCF-7 cells, while showing minimal effects on normal mammary epithelial cells. SEVs derived from PTA-treated cells maintained normal morphology and size but exhibited altered biological functions, selectively inhibiting the viability of MCF-7 cells. Further analysis revealed a significant downregulation of miR-21 in PTA-derived sEVs, suggesting a potential mechanism for the observed inhibitory effect. These findings indicate that PTA treatment may modulate sEV-mediated intercellular communication through miRNA regulation. Overall, this study provides new insights into the role of plasma-induced exosomal signaling in selective cancer inhibition and highlights its potential application in plasma-based cancer therapy.

Acknowledgements

The author DU Liyin was supported by Otsuka Toshimi Scholarship Foundation so she could focus on research. This work was partly supported by a Grant-in-Aid for Specially Promoted Research (No. 19H05462), a Grant-in-Aid for Scientific Research (B) (No. 21H01072), and a Grant-in-Aid for Scientific Research (A) (No. 24H00202) from the Ministry of Education, Culture, Sports, Science and Technology of Japan. Division for Medical Research Engineering, Nagoya University Graduate School of Medicine, provided access to the ultracentrifuge, TEM and their valuable technical support.

References

[1] “Cancer Over Time.” Accessed: Oct. 30, 2025. [Online]. Available: https://gco.iarc.fr/overtime

[2] H.-R. Metelmann *et al.*, “Clinical experience with cold plasma in the treatment of locally advanced head and neck cancer,” *Clinical Plasma Medicine*, vol. 9, pp. 6–13, Mar. 2018, doi: 10.1016/j.cpme.2017.09.001.

[3] H. Tanaka *et al.*, “Plasma-Activated Medium Selectively Kills Glioblastoma Brain Tumor Cells by Down-Regulating a Survival Signaling Molecule, AKT Kinase,” *PMED*, vol. 1, no. 3–4, 2011, doi: 10.1615/PlasmaMed.2012006275.

[4] D. B. Graves and G. Bauer, “Key Roles of Reactive Oxygen and Nitrogen Species,” in *Comprehensive Clinical Plasma Medicine: Cold Physical Plasma for Medical Application*, H.-R. Metelmann, T. von Woedtke, and K.-D. Weltmann, Eds., Cham: Springer International Publishing, 2018, pp. 71–82. doi: 10.1007/978-3-319-67627-2_4.

[5] “Reactive Oxygen Species in Plasma Medical Science (PAM and Cancer Therapy),” in *Plasma Medical Science*, Academic Press, 2019, pp. 249–318. doi: 10.1016/B978-0-12-815004-7.00005-6.

[6] M. L. Semmler *et al.*, “Molecular Mechanisms of the Efficacy of Cold Atmospheric Pressure Plasma (CAP) in Cancer Treatment,” *Cancers*, vol. 12, no. 2, Art. no. 2, Feb. 2020, doi: 10.3390/cancers12020269.

[7] H. Tanaka, S. Bekeschus, D. Yan, M. Hori, M. Keidar, and M. Laroussi, “Plasma-Treated Solutions (PTS) in Cancer Therapy,” *Cancers*, vol. 13, no. 7, p. 1737, Apr. 2021, doi: 10.3390/cancers13071737.

[8] H. Tanaka *et al.*, “Oxidative stress-dependent and -independent death of glioblastoma cells induced by non-thermal plasma-exposed solutions,” *Sci Rep*, vol. 9, no. 1, p. 13657, Sep. 2019, doi: 10.1038/s41598-019-50136-w.

[9] D. J. Stuehr, “Enzymes of the L-Arginine to Nitric Oxide Pathway,” *The Journal of Nutrition*, vol. 134, no. 10, pp. 2748S-2751S, Oct. 2004, doi: 10.1093/jn/134.10.2748S.

[10] S.-H. Kim, J. Roszik, E. A. Grimm, and S. Ekmekcioglu, “Impact of l-Arginine Metabolism on Immune Response and Anticancer Immunotherapy,” *Front. Oncol.*, vol. 8, Mar. 2018, doi: 10.3389/fonc.2018.00067.

[11] “Supplementation of l-arginine boosts the therapeutic efficacy of anticancer chemoimmunotherapy - Satoh - 2020 - Cancer Science - Wiley Online Library.” Accessed: Nov. 24, 2025. [Online]. Available: https://onlinelibrary.wiley.com/doi/10.1111/cas.14490?utm_source=chatgpt.com

[12] L. Du *et al.*, “Selective Killing of Human Breast Cancer Cells by Plasma-Treated L-Arginine Solution,” *Plasma Processes and Polymers*, vol. 22, no. 4, p. 2400192, 2025, doi: 10.1002/ppap.202400192.

[13] D. Liyin *et al.*, “Differential cytotoxicity of plasma-treated arginine in breast cancer

and normal cell lines: time-dependent effects and media-driven modulation," *Jpn. J. Appl. Phys.*, vol. 64, no. 9, p. 097002, Oct. 2025, doi: 10.35848/1347-4065/adfef0.

[14] D. M. Brizel *et al.*, "Elevated tumor lactate concentrations predict for an increased risk of metastases in head-and-neck cancer," *International Journal of Radiation Oncology*Biology*Physics*, vol. 51, no. 2, pp. 349–353, Oct. 2001, doi: 10.1016/S0360-3016(01)01630-3.

[15] G. Raposo and W. Stoorvogel, "Extracellular vesicles: Exosomes, microvesicles, and friends," *Journal of Cell Biology*, vol. 200, no. 4, pp. 373–383, Feb. 2013, doi: 10.1083/jcb.201211138.

[16] N. Kurake *et al.*, "Cell survival of glioblastoma grown in medium containing hydrogen peroxide and/or nitrite, or in plasma-activated medium," *Archives of Biochemistry and Biophysics*, vol. 605, pp. 102–108, Sep. 2016, doi: 10.1016/j.abb.2016.01.011.

[17] P. Raber, A. C. Ochoa, and P. C. Rodríguez, "Metabolism of L-Arginine by Myeloid-Derived Suppressor Cells in Cancer: Mechanisms of T cell suppression and Therapeutic Perspectives," *Immunol Invest*, vol. 41, no. 6–7, pp. 614–634, 2012, doi: 10.3109/08820139.2012.680634.

[18] C. Miron *et al.*, "Cancer-specific cytotoxicity of Ringer's acetate solution irradiated by cold atmospheric pressure plasma," *Free Radical Research*, vol. 57, no. 2, pp. 91–104, Feb. 2023, doi: 10.1080/10715762.2023.2201390.

[19] D. Ito *et al.*, "Cytotoxicity of plasma-irradiated lactate solution produced under atmospheric airtight conditions and generation of the methyl amino group," *Appl. Phys. Express*, vol. 15, no. 5, p. 056001, Apr. 2022, doi: 10.35848/1882-0786/ac6360.

[20] H. Tanaka *et al.*, "Plasma activated Ringer's lactate solution," *Free Radical Research*, vol. 57, no. 1, pp. 14–20, Jan. 2023, doi: 10.1080/10715762.2023.2182663.

[21] C. Miron *et al.*, "Cold Atmospheric Pressure Plasma-Activated Liquids for Cancer Treatment," in *Advances in Digital Health and Medical Bioengineering*, H.-N. Costin, R. Magjarević, and G. G. Petroiu, Eds., Cham: Springer Nature Switzerland, 2024, pp. 150–162. doi: 10.1007/978-3-031-62523-7_17.

[22] L. Du *et al.*, "Selective Killing of Human Breast Cancer Cells by Plasma-Treated L-Arginine Solution," *Plasma Processes and Polymers*, vol. n/a, no. n/a, p. e2400192, doi: 10.1002/ppap.202400192.

[23] T. Yamakawa *et al.*, "Effects of autophagy on the selective death of human breast cancer cells exposed to plasma-activated Ringer's lactate solution," *Free Radical Research*, vol. 58, no. 11, pp. 758–769, Nov. 2024, doi: 10.1080/10715762.2024.2433965.

[24] "Downregulation of Spry2 by miR-21 triggers malignancy in human gliomas | Oncogene." Accessed: Nov. 24, 2025. [Online]. Available: https://www.nature.com/articles/onc2010620

[25]H. Cheng *et al.*, “On the dose of plasma medicine: Plasma-activated medium (PAM) and its effect on cell viability,” *Physics of Plasmas*, vol. 29, no. 6, p. 063506, Jun. 2022, doi: 10.1063/5.0089357.

[26]G. Bauer, D. Sersenová, D. B. Graves, and Z. Machala, “Cold Atmospheric Plasma and Plasma-Activated Medium Trigger RONS-Based Tumor Cell Apoptosis,” *Sci Rep*, vol. 9, no. 1, Art. no. 1, Oct. 2019, doi: 10.1038/s41598-019-50291-0.

[27]A. G. Volkov, A. Bookal, J. S. Hairston, J. Roberts, G. Taengwa, and D. Patel, “Mechanisms of multielectron reactions at the plasma/water interface: Interfacial catalysis, RONS, nitrogen fixation, and plasma activated water,” *Electrochimica Acta*, vol. 385, p. 138441, Jul. 2021, doi: 10.1016/j.electacta.2021.138441.

[28]F. Kabeer *et al.*, “Single-cell decoding of drug induced transcriptomic reprogramming in triple negative breast cancers,” *Genome Biol*, vol. 25, no. 1, p. 191, Jul. 2024, doi: 10.1186/s13059-024-03318-3.

[29]S.-C. Lee *et al.*, “Chemotherapy-induced tumor gene expression changes in human breast cancers,” *Pharmacogenetics and Genomics*, vol. 19, no. 3, p. 181, Mar. 2009, doi: 10.1097/FPC.0b013e32831ebb5d.

[30]L. Garcia-Martinez, Y. Zhang, Y. Nakata, H. L. Chan, and L. Morey, “Epigenetic mechanisms in breast cancer therapy and resistance,” *Nat Commun*, vol. 12, no. 1, p. 1786, Mar. 2021, doi: 10.1038/s41467-021-22024-3.

[31]X. Xue *et al.*, “MiR-21 and MiR-155 promote non-small cell lung cancer progression by downregulating SOCS1, SOCS6, and PTEN,” *Oncotarget*, vol. 7, no. 51, pp. 84508–84519, Nov. 2016, doi: 10.18632/oncotarget.13022.

[32]“The Angiogenic Effect of microRNA-21 Targeting TIMP3 through the Regulation of MMP2 and MMP9 | PLOS One.” Accessed: Nov. 24, 2025. [Online]. Available: https://journals.plos.org/plosone/article?id=10.1371/journal.pone.0149537

[33]J. Dong, Y.-P. Zhao, L. Zhou, T.-P. Zhang, and G. Chen, “Bcl-2 Upregulation Induced by miR-21 Via a Direct Interaction Is Associated with Apoptosis and Chemoresistance in MIA PaCa-2 Pancreatic Cancer Cells,” *Archives of Medical Research*, vol. 42, no. 1, pp. 8–14, Jan. 2011, doi: 10.1016/j.arcmed.2011.01.006.

[34]I. A. Asangani *et al.*, “MicroRNA-21 (miR-21) post-transcriptionally downregulates tumor suppressor Pdcd4 and stimulates invasion, intravasation and metastasis in colorectal cancer,” *Oncogene*, vol. 27, no. 15, pp. 2128–2136, Apr. 2008, doi: 10.1038/sj.onc.1210856.

[35]M. Gao *et al.*, “SPRY2 loss enhances ErbB trafficking and PI3K/AKT signalling to drive human and mouse prostate carcinogenesis,” *EMBO Molecular Medicine*, vol. 4, no. 8, pp. 776–790, Aug. 2012, doi: 10.1002/emmm.201100944.

[36]C. Porta, C. Paglino, and A. Mosca, “Targeting PI3K/Akt/mTOR Signaling in Cancer,” *Front Oncol*, vol. 4, p. 64, Apr. 2014, doi: 10.3389/fonc.2014.00064.

[37] Y.-J. Guo, W.-W. Pan, S.-B. Liu, Z.-F. Shen, Y. Xu, and L.-L. Hu, "ERK/MAPK signalling pathway and tumorigenesis (Review)," *Experimental and Therapeutic Medicine*, vol. 19, no. 3, pp. 1997–2007, Mar. 2020, doi: 10.3892/etm.2020.8454.

[38] Z. Wang, H. Zhou, F. Cheng, Z. Zhang, and S. Long, "miR-21 Negatively Regulates the PTEN-PI3K-Akt-mTOR Signaling Pathway in Crohn's Disease by Altering Immune Tolerance and Epithelial-Mesenchymal Transition," *Discovery Medicine*, vol. 33, no. 170, pp. 153–166, Aug. 2022.

[39] J. Oh *et al.*, "The Membrane-Anchored MMP Inhibitor RECK Is a Key Regulator of Extracellular Matrix Integrity and Angiogenesis," *Cell*, vol. 107, no. 6, pp. 789–800, Dec. 2001, doi: 10.1016/S0092-8674(01)00597-9.

[40] "Regulation of matrix metalloproteinase-9 and inhibition of tumor invasion by the membrane-anchored glycoprotein RECK | PNAS." Accessed: Nov. 24, 2025. [Online]. Available: https://www.pnas.org/doi/abs/10.1073/pnas.95.22.13221

[41] M. W. Roomi, J. C. Monterrey, T. Kalinovsky, M. Rath, and A. Niedzwiecki, "Patterns of MMP-2 and MMP-9 expression in human cancer cell lines," *Oncology Reports*, vol. 21, no. 5, pp. 1323–1333, May 2009, doi: 10.3892/or_00000358.

[42] "Matrix metalloproteinases as diagnostic (MMP-13) and prognostic (MMP-2, MMP-9) markers of prostate cancer | Urolithiasis." Accessed: Nov. 24, 2025. [Online]. Available: https://link.springer.com/article/10.1007/s00240-004-0440-8

[43] "Molecular Pathways: Receptor Ectodomain Shedding in Treatment, Resistance, and Monitoring of Cancer | Clinical Cancer Research | American Association for Cancer Research." Accessed: Nov. 24, 2025. [Online]. Available: https://aacrjournals.org/clincancerres/article/23/3/623/80544/Molecular-Pathways-Receptor-Ectodomain-Shedding-in

[44] D. T. Chao and S. J. Korsmeyer, "BCL-2 FAMILY: Regulators of Cell Death," *Annual Review of Immunology*, vol. 16, no. Volume 16, 1998, pp. 395–419, Apr. 1998, doi: 10.1146/annurev.immunol.16.1.395.

[45] K. J. Campbell and S. W. G. Tait, "Targeting BCL-2 regulated apoptosis in cancer," *Open Biology*, vol. 8, no. 5, p. 180002, May 2018, doi: 10.1098/rsob.180002.

[46] "Feedback Regulations of miR-21 and MAPKs via Pdcd4 and Spry1 Are Involved in Arsenite-Induced Cell Malignant Transformation | PLOS One." Accessed: Nov. 24, 2025. [Online]. Available: https://journals.plos.org/plosone/article?id=10.1371/journal.pone.0057652

Abbreviation List

Abbreviation	Full Name

AC	Alternating Current
Ar	Argon
AKT	Protein kinase B
ADAM	A disintegrin and metalloproteinase
BAX	Bcl-2-associated X protein
BCL2	B-cell lymphoma 2
CAP	Cold atmospheric plasma
Ctrl	Control
Ctrl-sEVs	SEVs derived from untreated MCF-7 cells
DAPI	4′,6-diamidino-2-phenylindole
DMEM	Dulbecco's Modified Eagle Medium
DMEM (+)	Complete Dulbecco's Modified Eagle Medium
DMEM (-)	Serum-free Dulbecco's Modified Eagle Medium
EGFR	Epidermal growth factor receptor
ERK	Extracellular signal-regulated kinase
EVs	Extracellular vesicles
FBS	Fetal bovine serum
HER2	Human epidermal growth factor receptor 2
JNK	c-Jun N-terminal kinase
MAPK	Mitogen-activated protein kinase
MEGM	Mammary Gland Epithelial Cell Growth Medium Bullet Kit
MTS	3-(4,5-Dimethylthiazol-2-yl)-5-(3-Carboxymethoxyphenyl)-2-(4-Sulfophenyl)-2H-Tetrazolium
MCF-7	Michigan Cancer Foundation-7 breast cancer cell line
MCF-10A	Human mammary epithelial cell line

miRNA	MicroRNA
MMP	Matrix metalloproteinase
MTS	3-(4,5-dimethylthiazol-2-yl)-5-(3-carboxymethoxyphenyl)-2-(4-sulfophenyl)-2H-tetrazolium
NTA	Nanoparticle tracking analysis
PBS	Phosphate-buffered saline
PDCD4	Programmed cell death protein 4
PI3K	Phosphoinositide 3-kinase
PTA	Plasma-treated L-arginine solution
PTA-sEVs	sEVs derived from PTA-treated MCF-7 cells
P/S	Penicillin-Streptomycin
PFA	Paraformaldehyde
qRT-PCR	Quantitative reverse transcription polymerase chain reaction
RONS	Reactive oxygen and nitrogen species
ROS	Reactive oxygen species
SPRY2	Sprouty homolog 2
slm	Standard Liters Per Minute
TEM	Transmission electron microscopy
TIMP3	Tissue inhibitor of metalloproteinase 3
U6	U6 small nuclear RNA
VEGFR	Vascular endothelial growth factor receptor